PAPER • **OPEN ACCESS**

Confinement creates a 9 GPa ambience: emergence of cristobalite phases in a silica film

To cite this article: Subrata Pramanik *et al* 2021 *Mater. Res. Express* **8** 066403

View the article online for updates and enhancements.

You may also like

- Electroanalytical Quantification of Electrolyte Transport Resistance in Porous Electrodes
Wenxiu Wang, Daniel Juarez-Robles and Partha P. Mukherjee
- 11th International Conference on X-ray Microscopy (XRM2012)
Hongjie Xu, Ziyu Wu and Renzhong Tai
- Low-*k* films modification under EUV and VUV radiation
T V Rakhimova, A T Rakhimov, Yu A Mankelevich et al.

This content was downloaded from IP address 14.139.222.10 on 15/12/2021 at 05:44

Materials Research Express

PAPER

Confinement creates a 9 GPa ambience: emergence of cristobalite phases in a silica film

Subrata Pramanik[1], **Jiten Ghosh**[1], **Dipak Kumar Chanda**[1], **Mrinmay Kumar Mukhopadhyay**[2] and **Alokmay Datta**[1,*]

[1] XRD and SEM Units, Material Characterization and Instrumentation Division, CSIR-Central Glass and Ceramic Research Institute, 196 Raja Subodh Chandra Mullick Road, Kolkata 700 032, India
[2] Surface Physics and Materials Science Division, Saha Institute of Nuclear Physics, 1/AF Bidhannagar, Kolkata 700 064, India
* Author to whom any correspondence should be addressed.

E-mail: fellow1@cgcri.res.in

Keywords: silica film, cristobalite phase, XRD, XPS, SIMS, FE-SEM, x-ray reflectivity

OPEN ACCESS

RECEIVED
17 October 2020

REVISED
3 April 2021

ACCEPTED FOR PUBLICATION
24 May 2021

PUBLISHED
2 June 2021

Original content from this work may be used under the terms of the Creative Commons Attribution 4.0 licence.

Any further distribution of this work must maintain attribution to the author(s) and the title of the work, journal citation and DOI.

Abstract

We present here the results of the x-ray fluorescence (XRF), x-ray photoelectron spectroscopy (XPS), Field Emission Scanning Electron Microscopy (FESEM) and Energy Dispersive Analysis of x-rays (EDAX), x-ray Reflectivity (XRR), Secondary Ion Mass spectroscopy (SIMS) and x-ray Diffraction (XRD) studies of silica films spin-coated from a Tetraethyl Orthosilicate (TEOS) precursor on native and hydrophilized Al substrates. It is observed that the substrates are mainly porous (porosity $\sim$ 33%) AlO(OH), there is a diffuse interlayer of highly porous (porosity $\sim$ 90%) AlO(OH), essentially a modification of the substrate, and a top layer of silica composed of nanocrystals with in-plane dimensions of 100–300 nm and thickness of 2.5 nm with a sharply defined silica-hydrated alumina interface. The silica nanocrystals were found in the metastable high pressure cristobalite phases with the tetragonal or α-phase co-existing in its low (0.77 GPa) and high (9 GPa) pressure structures. This indicates a high normal stress developed from the confinement and provides a basis for the quantitative assessment of the confinement force, which comes out to be higher in value than the van der Waals force but weaker than the Hydrogen bonding force.

1. Introduction

Observation of the evolution of order in simple and complex fluids [1–5] under confinement, as obtained in thin films of these materials, and the striking changes in the physical properties due to such ordering have opened some new areas of research, most notably in the thermal properties of such 'nanoconfined liquids'[6, 7]. The most important physical quantity to emerge from the studies is the 'confinement force'[8] working along the direction of confinement and increasing with the decrease in the film thickness [9]. The effect of this force on liquids and other soft, amorphous materials is, as expected, a preferred blocking of degrees of freedom in that direction that lowers the entropy, giving rise to the observed evolution of order.

Similarly, the effect of the confinement on the growth of crystalline phases has generated intense interest during the last decade [10–13]. Some studies have focused on the growth of nanocrystals, especially crystalline nanorods of selected metal oxides, confined in oriented nanoporous matrices, where the pores have high aspect ratios and are organized in arrays [10, 11]. The major results of these efforts are the growth of new polymorphic phases and the stabilization of intermediate metastable phases, both controlled by pore-size and orientation of the pores relative to substrates that are epitaxially matched with the crystalline phases of the nanorods. Besides confinement as the major determinant of the stabilization of metastable phases, the very high surface-to-volume ratio of the nanopores supplies a large free energy to enable the growth of phases not achieved in the bulk.

For growth of a crystal on a flat surface, the role of a nanofilm of the liquid (solution or melt) providing material for the growth, confined between the crystal and the substrate has been investigated through *in silico* studies [12]. Viscosity of this film was found to ensure continuous formation of the crystal whereas the attraction

© 2021 The Author(s). Published by IOP Publishing Ltd

between the crystal and substrate surfaces make discontinuous cavities in the liquid film. Surface force measurements between two similar surfaces with a film of salt solution confined between them indicated an internal repulsive force to develop when the film thickness goes below 1 μm, which leads to a metastable amorphous and viscous phase [13].

In contrast to these studies on growth under confinement between identical or at least strongly interacting interfaces, we would like to probe the apparently simpler case of confinement between the air-film and film-substrate interfaces. This involves structural investigations on materials with known crystalline phases grown from precursors, on a suitable substrate, as ultrathin films of gradually decreasing thickness. This is required to (1) see whether novel crystalline phases appear during growth under nanoconfinement and, equally or even more important (2) an estimate of the energy corresponding to the confinement force. The latter is estimable from either the bulk growth conditions, in particular the temperature and pressure, of known phases that may appear during growth under confinement, or from the bond enthalpy of such phases. We are initiating the study on growth of crystalline phases of silica under nanoconfinement to probe both these aspects.

Oxides of Si are the most abundant minerals in the Earth crust but in a number of crystalline and amorphous forms including quartz, tridymite, cristobalite, coesite, stishovite, and several others with a very rich and complex phase space [14–17]. The basic constituent in almost all these minerals is the tetrahedral SiO_4 unit arranged in different ways but the complexity arises from the fact that the bond lengths and the bond angles may vary considerably to allow for a variety of packing. Compared to the extensive studies on the bulk phases of silica, the data on nanostructure is sparse. However, a recent study on the formation of nanoparticles in the dominant α-quartz phase under ambient conditions has shown efficiency of confinement in generating this silica phase that can be grown only under high temperature and pressure [18]. We have commenced a similar series of studies here with thickness in the nanometer scale.

We have spin-coated the silica films from a solution of a silica precursor and a suitable reductant on native and hydrophilized Al surfaces as Al^{3+} ions have been shown to play a role in the transition of the high temperature phases of silica [19]. While the substrates were found to be porous hydrated alumina with a highly porous modified layer on top, the silica film in both cases was found to be composed of isolated nanocrystals with very high in-plane/out-of-plane aspect ratio. They were found in high pressure and low density cristobalite phases where the tetragonal or α-phase co-existing in its low (0.77 GPa) and high (9 GPa) pressure structure and at the ambient conditions. The crystal domain size ~147 Å as extracted from the peaks. Comparison with the bulk conditions of growth of cristobalite phases gives an idea of the lower limit of the energy corresponding to the confinement force.

2. Experimental details

2.1. Silica film preparation

Silica was prepared by the reduction of the silica precursor Tetraethyl Orthosilicate (TEOS) by methanol in presence of acetic acid as stabilizer against SiOx precipitate. 3 ml of TEOS was dissolved in 30 ml of methanol and a few drops of acetic acid were added. This solution was stirred for 2 h under ambient conditions at the rate of 600 rpm. Then 10 ml of the solution was spin-coated on the native Al substrate at the rate of 3000 rpm for 25 s and dried overnight to obtain the thin film on native Al substrate (sample 1).

To make silica thin film on hydrophilized Al (sample 2), the Al substrate was first treated with (N/20) NaOH and dried. The same procedure is then followed for obtaining the film.

2.2. X-ray fluorescence spectroscopy

The qualitative elemental analysis of the hydrophilized film was done by x-ray fluorescence (XRF) spectroscopy. XRF spectroscopy of the silica film on hydrophilized Al substrate was done using Axios Panalytical XRF Spectrometer.

2.3. X-ray photoelectron spectroscopy

The elemental composition and the electronic states of the elements present in the native sample (sample 1) were determined by x-ray photoelectron spectroscopy (XPS). XPS of the sample was performed in a PHI 5000 VERSAPROBE II scanning microprobe (Physical Electronics, USA) with Al K_α (1486.6 eV) x-ray source operating at 15 kV and 25 W, and with probe size of 10 μm. Collected XPS peak profiles were fit with the required combinations of Gaussian functions.

2.4. Field emission scanning electron microscopy

The morphology of synthesized thin films was studied by FESEM (Model Supra VP35, Carl Zeiss, Germany) at an applied high tension of 10 keV to obtain images at 50000 $\times$ and 65000 $\times$ for sample 1 and sample 2, respectively. The typical elemental composition of the thin films was obtained by energy dispersive analysis of x-rays (EDAX) in the same instrument.

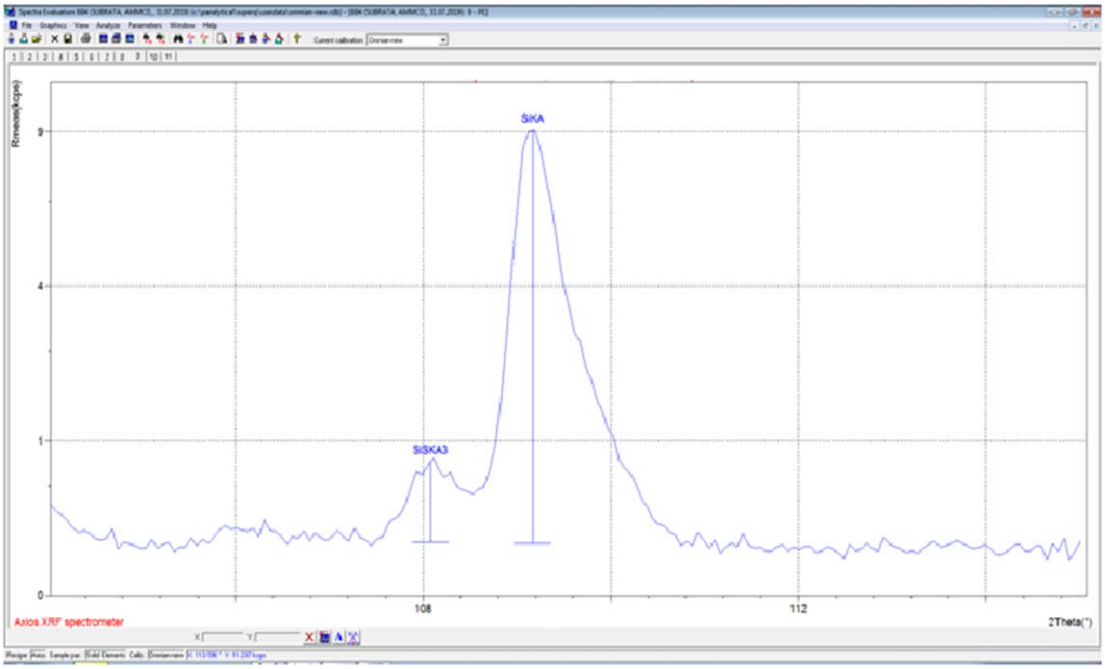

Figure 1. X-Ray Fluorescence (XRF) Spectra of Sample 2 showing presence of Al, Si, O, and trace amount of Na.

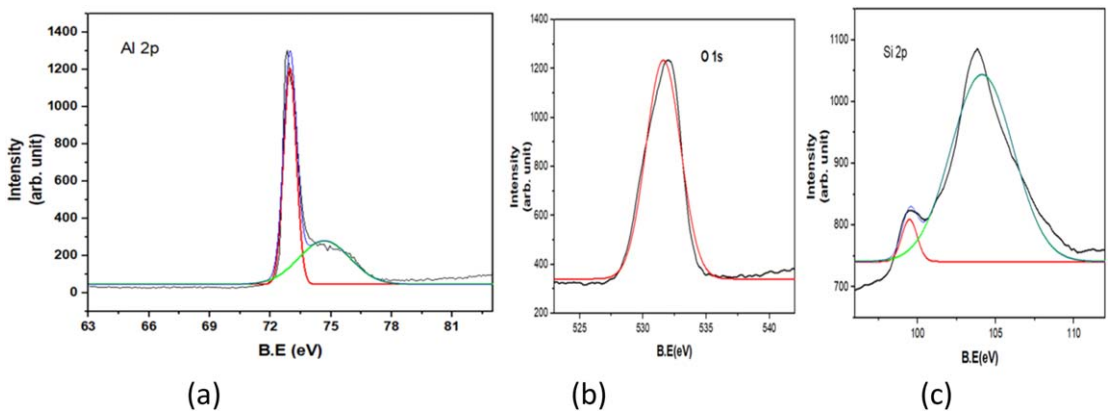

Figure 2. X-ray photoelectron spectra of silica coated native Al substrate on its surface at (a) 2p state of Al (b) 1 s state of O (c) 2p state of Si. Individual peaks fit with Gaussian functions in green and the overall peak profiles fit with the convolution of the functions (red).

2.5. X-ray reflectivity

The x-ray Reflectivity data of the samples were collected using the Cu K_α (wavelength $\lambda = 1.54$Å) radiation from a sealed tube source in a Rigaku Diffractometer for the thickness, average electron density and roughness measurements.

2.6. Secondary ion mass spectroscopy

Secondary ion mass spectroscopy (SIMS) for the surface analysis of the samples was carried out using a quadruple mass spectrometer-based SIMS instrument (HIDEN Analytical Ltd, UK). The base pressure was of the order of 2.3×10^{-7} mbar. The samples were investigated with 3 keV O^{2+} primary ions with 23 nA current.

2.7. X-ray diffraction

The structure and the crystallographic phase determination of the thin film samples were done using x-ray diffraction. The x-ray diffraction patterns of the films were recorded in ULTIMA IV x-ray Diffractometer (Rigaku) operating at 40 kV and 40 mA using Cu K_α radiation. The XRD data were recorded with step size 20 mdeg (2θ) and step time 1 s from 10° to 90° for these films.

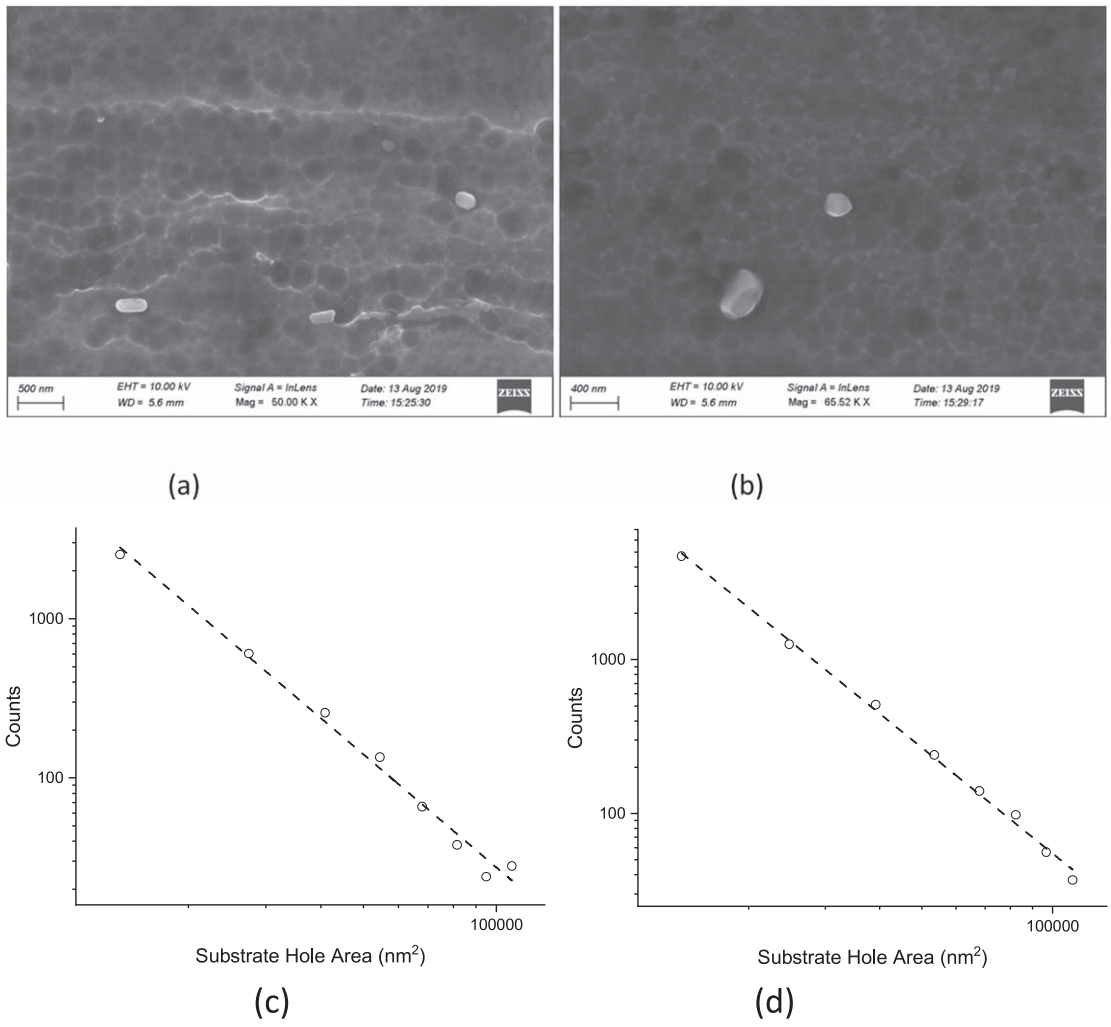

Figure 3. Field Emission Scanning Electron Microscopy images of silica spin-coated on (a) native and (b) hydrophilized Al substrates. Log-log plots of counts of holes (pores) of different areas in the (c) native Al and (d) hydrophilized Al substrate as functions of the hole area.

Table 1. Electronic states of elements in silica film and native aluminium substrate from spectroscopy.

State	Binding energy (eV)	Assignment
Al 2p	72.969, 74.67	Al $2p_{3/2}$ (73.0 eV), Al $2p_{1/2}$ (72.7 eV) Al_2O_3(74.6 eV)
O 1 s	532.62	O 1 s (532.9 eV in SiO_2)
Si 2p	99.52, 104.17	Si $2p_{3/2}$ (99.4 eV in Si element), Si 2p (103.5 eV in SiO_2)

Table 2. Parameters of the two-layer model used to calculate the reflectivity profile of sample 2.

Thickness (nm)	Average electron density (ε nm^{-3})	Interfacial roughness (nm)
2.56	400	1.5
8.90	16	0.3

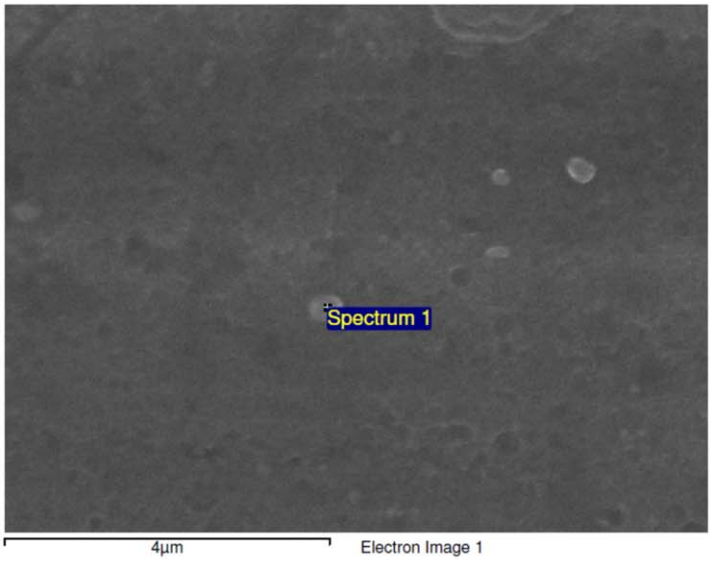

(a)

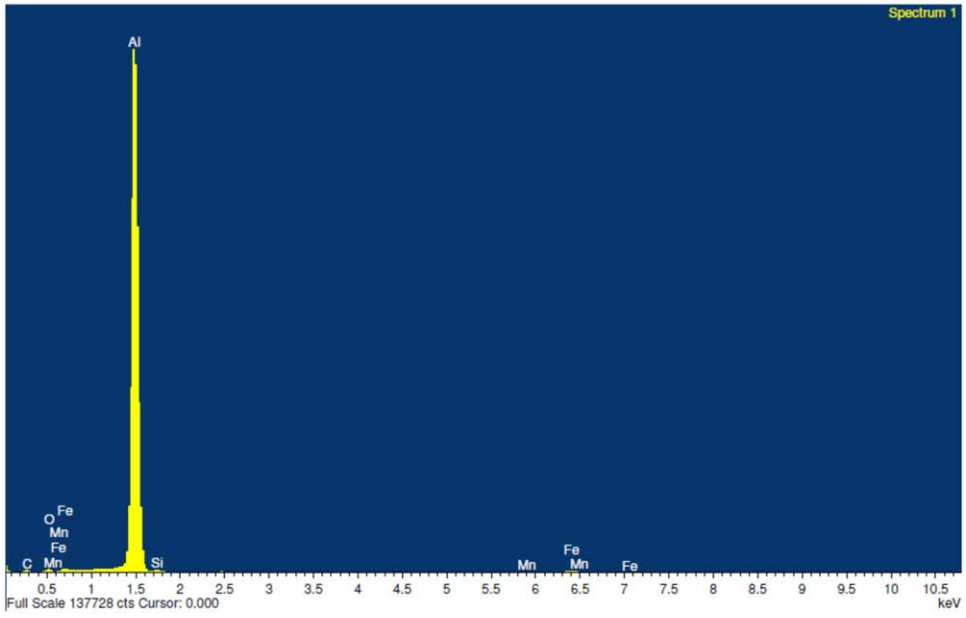

(b)

Figure 4. Energy Dispersive Analysis of x-rays (EDAX) spectroscopy of (a) silica spin-coated on hydrophilized Al substrate with (b) showing the element analysis of the spot marked in (a).

3. Experimental results

3.1. X-ray fluorescence and photoelectron spectroscopy: film composition

XRF spectra shows the presence of Al, O, Na and Si. The presence of silica is confirmed from the XRF spectra and shown in figure 1. The trace amount of Na observed comes from the NaOH used to hydrophilize the Al substrate (table 1).

Collected XPS peak profiles were fit with the required combinations of Gaussian functions.

Figure 2 and table 2 summarize the results of XPS analysis. The data shows peaks in the 70–80 eV, 530–533 eV and 90–105 eV ranges, corresponding to the 2p band of Al, 1 s band of O and 2p band of Si respectively. The two peaks in the first range, namely 72.969 eV and 74.67 eV can be assigned to Al $2p_{3/2}$ in pure Al metal state and Al_2O_3 respectively, providing evidence of the formation of a layer of Aluminium oxide on the Al substrate. In the second range, the peak at 532.6 eV corresponds to the O 1 s state in SiO_2 in the cristobalite phases and in the third

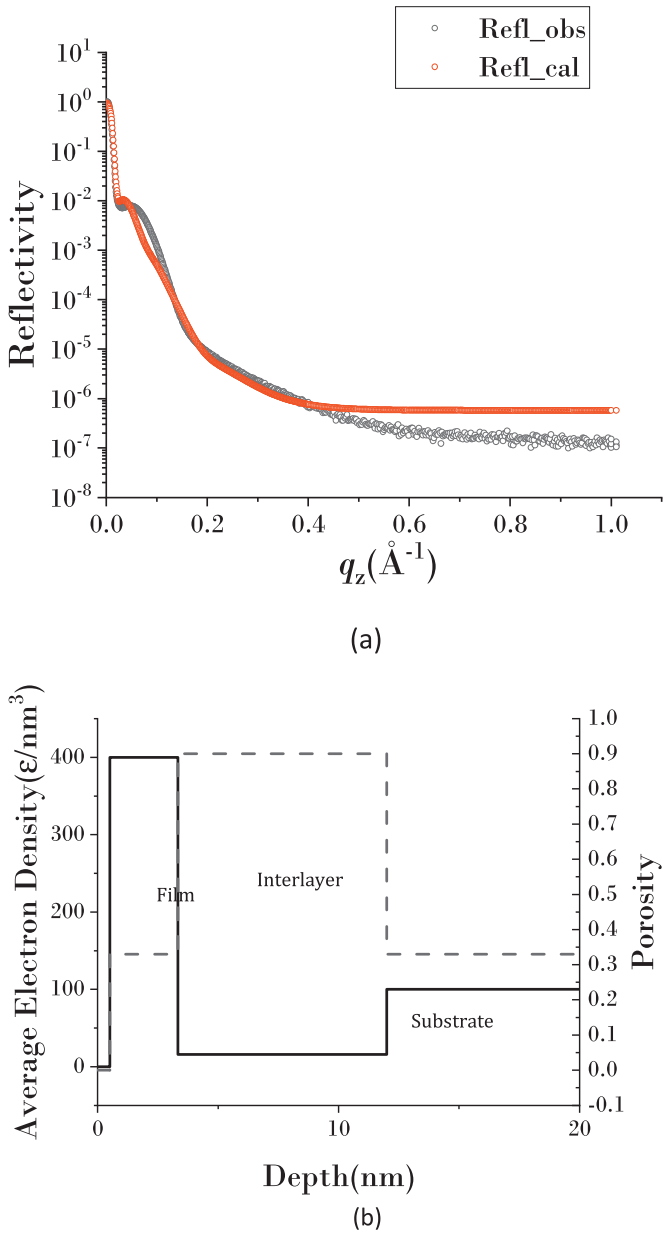

Figure 5. X-ray reflectivity profile (data in open black circles, a) and Electron Density Profile (line, b) of silica film on hydrophilized substrate built from the thickness and average electron density (aed) values (table 2) from the two-layer model that generates the reflectivity profile (open red circles) in (a). The porosity profile in (b) is generated by considering the aed of film to be that of silica ($600\varepsilon/Å^3$) and that of the interlayer and substrate to be that of AlO(OH) ($150\varepsilon/Å^3$).

range, the two peaks at 99.52 eV and 104.17 eV correspond to, respectively, the Si $2p_{3/2}$ of elemental Si and Si 2p state of SiO_2 cristobalite phase [20].

3.2. Field emission scanning electron microscopy: in-plane morphology

Images obtained from FESEM of samples 1 and 2 are shown in figure 3(a) and (b), respectively. Both show scattered nanocrystals on a highly porous background. The images were analysed using the ImageJ Freeware of the National Health Service (NHS), USA. The dimensions of the crystals of sample 1 lie between 100 nm and 300 nm, while those of sample 2 lie between 200 nm and 400 nm. The results of EDAX carried out on a spot located on a randomly selected nanocrystal (a) of sample 2 are shown in (b) of figure 4. As expected, the dominant composition is Al indicating the substrate. However, the next strongest signals are from Si and O, confirming the composition of the nanocrystals to be some oxide of silicon.

It is apparent from the FESEM images that the Al substrates in both samples have high porosity. In fact, the porosity is around 70% in both cases. Also, the area of the pores falls within the 14000 nm^2–100000 nm^2 range with those with the lowest area having the dominant (~80%) fraction. The probability P (given by the counts in

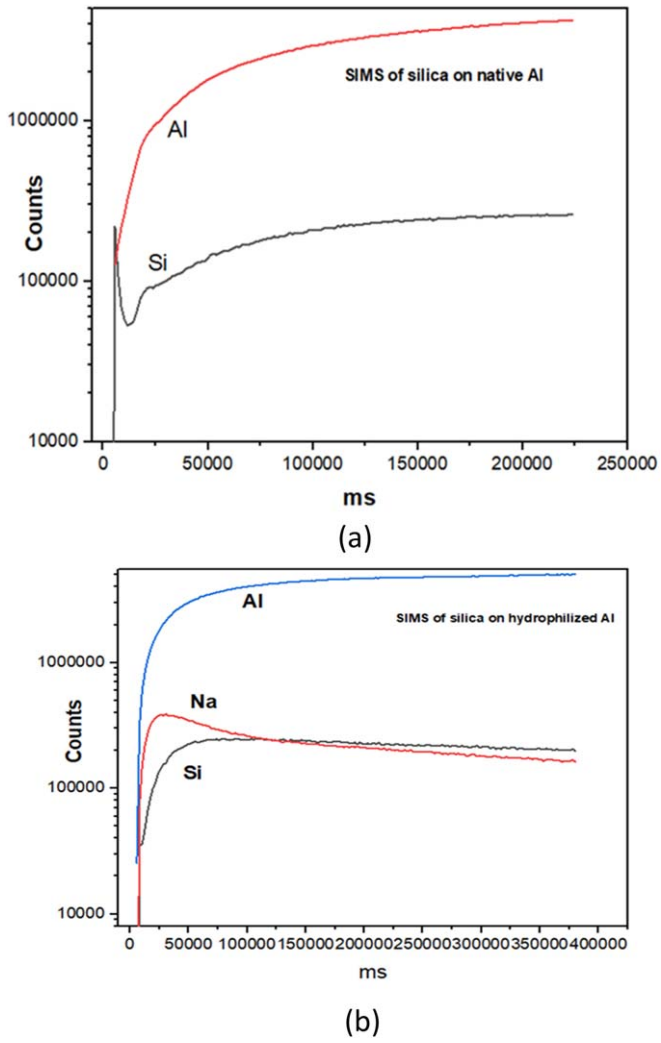

Figure 6. Secondary Ion Mass Spectroscopy of the samples (a) silica on native Al and (b) silica on hydrophilized Al. Al, Si signals are shown in case of native sample and along with them Na signal is shown in case of hydrophilized sample.

figure 3(c) and (d)) of a pore having area A has a functional dependence on A given by $P = kA^p$, with $p = -2.41$ for sample 1, and $p = -2.29$ for sample 2.

3.3. X-ray reflectivity: electron density profile along film thickness

Specular reflectivity profile, i.e., Reflectivity as a function of q_z (component of scattering vector normal to sample surface, $q_z = (4\pi/\lambda)\sin\theta, \theta =$ incident angle) of the sample on hydrophilized Al substrate is shown (black open circles) in figure 5(a). A two-layer model with the parameters given in table 2, used in the Parratt analysis scheme [21], generated the profile shown in red open circles in this figure, is satisfactory within the data quality. The electron density profile of the three-layer model, with average electron density (aed) and thickness values from table 2, is shown in figure 5(b). The interfacial roughness (ρ) denotes the width of the error function used to model the interface. The aed of the substrate and the film-substrate ρ came out to be 100 ε nm^{-3} and 2 nm, respectively.

3.4. Secondary ion mass spectroscopy: distribution profile

The results of SIMS studies on sample 1 (native) and sample 2 (hydrophilized) are summarized in figure 6(a) and (b) respectively. Due to the lack of flatness of the sample surfaces, the craters created by the ion beam could not be measured accurately and thus the spectra are plotted against the time of irradiation of the samples by the ion beams (in ms) instead of the depth of the mass species from the surface. The depth is proportional to the time.

From figure 6(a) it is shown that silica layer sits on the top of the native Al substrate with a depleted layer beneath mixed the alumina (Al_2O_3) layer which is obvious from XPS study. From figure 6(b) for the hydrophilized substrate there is penetration of the silica and extended mixing with the alumina. The presence of sodium in the substrate due to the use of Na for the preparation of hydrophilized Al substrate.

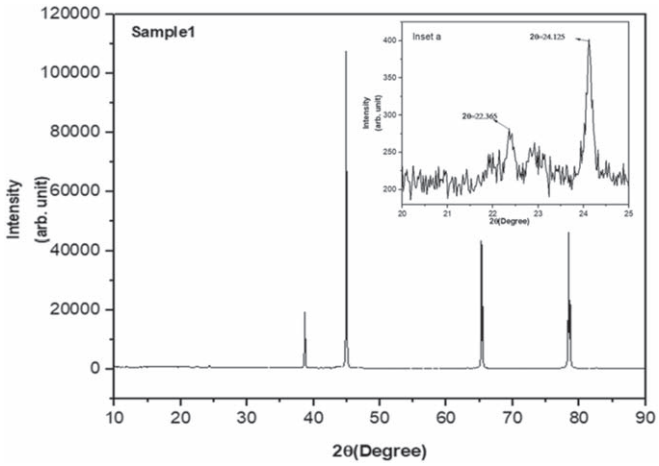

Figure 7. X-ray diffraction pattern recorded for silica film on native Al substrate. Inset: assigned peaks of the cristobalite from (100) and (101) plane repectively. See text for details.

3.5. X-ray diffraction: crystalline phases

From figure 7 for the film on the native Al substrate, the strong Bragg peaks in the XRD pattern comes from the cubic Al with a = b = c = 4.0634 Å. The weak but clear peaks (inset) at 22.365° and 24.125° could be assigned to the reflections from the (100) plane of the low-pressure (0.77 GPa) [14] and from the (101) plane of the high-pressure (9 GPa) [16] α-cristobalite phase of silica, respectively. Both phases have tetragonal structures with a = b = 4.898Å, and c = 6.130 Å for the high pressure α-cristobalite phase and a = b = 4.898Å, c = 6.768Å for the low pressure α-cristobalite phase. This result of the XRD analysis of sample 1 is summarized in the table 3.

On the other hand for the film on hydrophilized Al substrate, the main peaks in figure 8 are due to AlO(OH) in an orthorhombic phase with a = 4.7128Å, b = 4.2221Å, c = 2.8315Å. The presence of the 0.77 GPa and the 9 GPa α-cristobalite phases are reproduced by the presence of the (100) and (101) reflections (inset), respectively. The presence of these phases are confirmed in figure 9 by the higher order reflections peaks at 58.151° (301) (inset c) and 69.479° (221) (inset d) corresponding to the 0.77 GPa and 9 GPa structures, respectively. These XRD results for the hydrophilized sample or sample 2 are summarized in table 4.

4. Discussions

4.1. Film composition and structure

XREF, XPS, FESEM, EDAX, XRD and SIMS we find that the sample consists of silica nanocrystals of in-plane dimensions of 100–400 nm and aspect ratio 2–3, sitting on a substrate. The substrate is composed alumina, most probably hydrated, having a porosity of nearly 0.7, as averaged over the normal to the substrate (FESEM has very poor resolution along this direction), and with a distribution of pore sizes dominated strongly by the smallest pores of diameter ($\sim$ 130 nm).

From XRR, we find that the sample can be modeled as a two-layer film sitting on a AlO(OH) substrate with 33% porosity, where the top layer electron density matches with silica with 33% porosity and a large roughness, of nearly half the layer thickness, beween the layer and air, both consistent with isolated nanocrystals. The thickness of this layer $\sim$ 2.5 nm, hence the nanocrystals have very high (40–160) length-to-thickness ratios. The next layer has a thickness $\sim$ 8.9 nm and its electron density matches with AlO(OH) with 90% porosity. It has a sharp interface with the silica layer and a very diffuse interface with the substrate. Hence the porosity of this layer and that of the substrate average out along the normal to yield the value given by FESEM.

We have summarized these results in the schematic model presented in figure 10. It is clear that the second layer obtained from XRR is in fact a highly porous diffuse modification of the Al substrate, itself modified to hydrated alumina. The silica nanocrystals have a dimension of only a few lattice constants normal to the substrate.

4.2. The cristobalite phase

Cristobalite is one of the most widely studied silica phases or, to be more precise, family of phases. However, the cristobalite phase space is itself quite complicated due to existence of metastable phases with a continuous range

Table 3. Assigned x-ray diffraction peaks of the silica film on native Al substrate.

Sample name	Main Bragg peaks (Substrate)	Peaks of cristobalite			
		Peak position (2θ)	Assignments/crystallograpghic plane	Phases Of cristobalite	Unit cell parameters
Silica On Native Al (Sample 1)	Main peaks are predominantly due to Al, Cubic phase. a = b = c = 4.0634Å	22.365°	(100)	Low pressure α-cristobalite phase, Tetragonal	a = b = 4.898Å, c = 6.768Å
		24.125°	(101)	High pressure α-cristobalite phase, Tetragonal	a = b = 4.599Å, c = 6.130Å

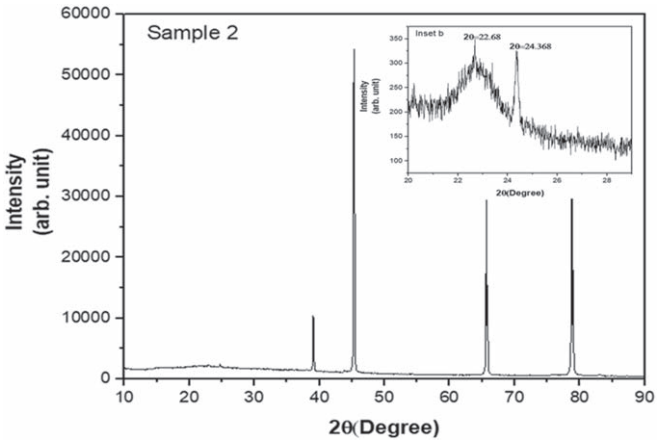

Figure 8. X-ray diffraction pattern for the silica on hydrophilized Al substrate. Inset: assigned peaks of cristobalite from (100) and (101) plane repectively. See text for details.

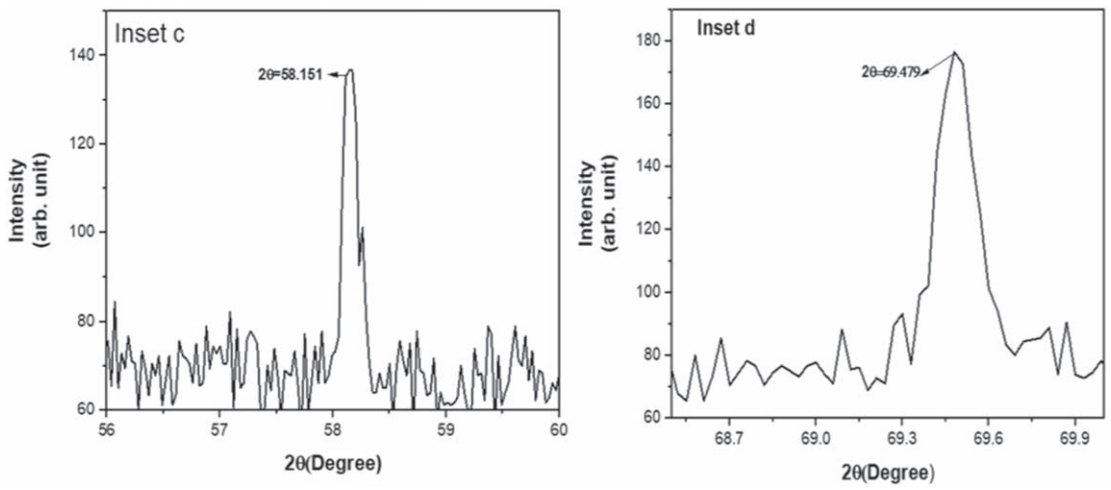

Figure 9. Close-up views of assigned peaks of cristobalite on hydrophilized Al substrate at 58.151°(301) (Inset c) and 68.479° (221) (Inset d). See text for details.

of lattice parameters over a large range of temperature and pressure. Again it has been predicted [22] and found [16] that some of the transitions among the cristobalite phases depend on the compression rate.

The stable ambient pressure (∼ 0.1 GPa), high temperature (1743 K) phase is the cubic β-cristobalite phase with eight SiO_4 tetrahedra in its unit cell. This phase becomes metastable as the temperature is lowered till, at around 440 K [19], it goes into the metastable tetragonal α-cristobalite phase with a much smaller unit cell having four SiO_4 tetrahedra.

The α-cristobalite phase has a continuous range of structures over pressures ranging from ambient to 1.8 GPa where the Si-O bond length remains constant at around 1.6 Å and the Si-O-Si bond angles of the SiO_4 tetrahedra varying within 108° and 111° but the Si-O-Si bond angle between two corner-sharing tetrahedra varying continuously from 146.49° to 140.4° thus changing the packing [14]. Under slow compression, at around 1.8 GPa α-cristobalite transforms to another stable phase, the monoclinic cristobalite-II [22]. However, under fast compression, the α-cristobalite phase could be maintained till 10 GPa with a inter-tetrahedral Si-O-Si angle further reduced to 127.8° at 9.1 GPa [16].

In our silica film, we have found the α-cristobalite phases that form in bulk at 0.77 and at 9.1 GPa and at around 440 K. The corresponding cell volumes are 162.4 $Å^3$ and 129.6 $Å^3$, the aspect ratios (c/a) are 1.38 and 1.33, and the inter-tetrahedral Si-O-Si angles are 142.1° and 127.8°. Hence the effect of confinement is seen to be like producing a very high pressure and moderately high temperature environment. It is also apparent that there is an enormous pressure gradient present in the film (∼ 9 GPa over 200 Å). Since the aspect ratio is not changing significantly over this huge pressure range, this pressure is most probably equally active over all the cell faces. It is also to be noted that confinement is giving rise to metastable phases of silica, similar to its effect in giving rise to a one-dimensionally ordered, metastable phase in polystyrene [4].

Table 4. Assigned x-ray diffraction peaks of the silica film on hydrophilized Al substrate.

Sample name	Main Bragg peaks (Substrate)	Peaks of cristobalite			
		Peak position (2θ)	Assignments crystallograpghic plane	Phases	Unit cell parameters
Silica on hydrophilized Al substrate (Sample 2)	Main peaks are due to	22.68°	(100)	Low pressure α-cristobalite phase, Tetragonal	a = b = 4.898Å, c = 6.768Å
	AlO(OH),	24.368°	(101)	High pressure α-cristobalite phase, Tetragonal	a = b = 4.599Å, c = 6.130Å
	Orthorhombic phase, a = 4.7128Å	58.151°	(301)	Low pressure α-cristobalite phase, Tetragonal	a = b = 4.898Å, c = 6.768Å
	b = 4.2221Å c = 2.8315Å	69.479°	(221)	High pressure α-cristobalite phase, Tetragonal	a = b = 4.599Å, c = 6.130Å

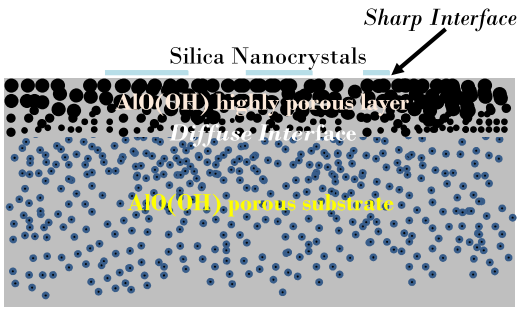

Figure 10. Schematic diagram of the samples constructed on results obtained from XREF, XPS, FESEM,EDAX, XRR, and SIMS. From bottom upwards the layers are, Al, AlO(OH) with low porosity (small pores), AlO(OH) with high porosity (large pores), and SiO_2.

4.3. The confinement force: probable cause and estimate

As we have found, the silica nanocrystals formed in the spin-coating process have large dimensions in the plane of the substrate but thickness only about a few times the lattice constants of the silica crystalline phases. Also, the interface between these crystals and the substrate is very sharp. The very high degree of confinement normal to the substrate and the high potential barrier presented by the sharp interface lead to a large confinement force.

Two other points are to be noted. The high porosity of the modified AlO(OH) substrate gives rise to a very large interfacial free energy [11]. This can add to the free energy equivalent of a high pressure and temperature ambience. Again, the lattice constants of AlO(OH) (in contrast to Al) being closer to those of the cristobalite phases, is more likely to reduce the interfacial stress. This gains relevance from the fact that the high pressure phase, with lattice constants closer to AlO(OH), is observed only on the hydrophilized substrate.

From the structural data of the phases, especially that corresponding to the bulk α-cristobalite phase at 9.1 GPa, we can estimate the average forces acting on the *ab*, *bc*, and *ca* faces to be around 1.9 pN, 2.5 pN, and 2.5 pN, respectively. This is about an order lower than the hydrogen bonding force between a host and a guest molecule [23]. In absence of direct measurement of van der Waals force between silica crystallites, we can compare the energy of van der Waals interaction between silica particles across water ($\sim 10^{-23}$ J $- 10^{-22}$ J) and a rough estimate of the energy corresponding to the confinement force ($\sim 10^{-21}$ J) and find the latter to be about one order of magnitude higher than the former.

5. Conclusions and outlook

We have carried out x-ray Fluorescence Spectroscopy, x-ray Photoelectron Spectroscopy, Field Emission Scanning Electron Microscopy and Energy Dispersive Analysis of x-rays, x-ray Reflectivity, Secondary Ion Mass Spectroscopy, and x-ray Diffraction studies on silica films spin-coated on native and hydrophilized Al substrates under ambient conditions from TEOS precursor reduced by methanol. Each sample was found to consist of a layer of ultrathin nanocrystals of silica on a highly porous layer of hydrated alumina, a modification of a porous AlO(OH) substrate. Weak but clear peaks of silica were observed that could be assigned to the high temperature and high pressure metastable α-cristobalite phase with structures corresponding to those at 0.77 and 9.0 GPa. These observations provide us with a quantitative estimate of the confinement force, whose value falls between those of the van der Waals force and the Hydrogen bonding force.

Acknowledgments

SP thanks Department of Atomic Energy for granting Research Fellowships. AD thanks the Department of Atomic Energy for awarding the Raja Ramanna Fellowship. We would like to thank Director CSIR-CGCRI for giving the permission to publish this work.

Data availability statement

All data that support the findings of this study are included within the article (and any supplementary files).

ORCID iDs

Alokmay Datta https://orcid.org/0000-0002-2542-1042

References

[1] Yu C-J, Richter A G, Datta A, Durbin M K and Dutta P 1999 *Phys. Rev. Lett.* **82** 2326
[2] Sanyal M K, Basu J K, Datta A and Banerjee S 1996 *Europhys. Lett.* **36** 265
[3] Yu C-J, Richter A G, Datta A, Durbin M K and Dutta P 2000 *Physica B* **283** 23
[4] Chattopadhyay S and Datta A 2005 *Physical Review B* **72** 099539
[5] Anaredy R S and Shaw S K 2018 *J. Phys. Chem. C* **122** 19731
[6] Jiang H, Xu Q, Huang C and Shi L 2015 *Appl. Phys. A* **118** 197
[7] Ambreen T and Kim M-H 2018 *Renewbl. Sustainbl. Energy Rev.* **91** 564
Taha-Tijerina J J 2018 Thermal transport and challenges on nanofluids performance *Microfluidics and Nanofluidics* ed M S Kandelousi (London: IntechOpen) ch 9
[8] Chattopadhyay S, Datta A, Giglia A, Mahne N, Das A and Nannarone S 2007 *Macromolecules* **40** 9190
[9] Xiang L, Zhang J, Gong L and Zeng H 2020 *Soft Matter* **16** 6697
Erdős M, Galteland O, Bedeaux D, Kjelstrup S, Moultos O A and Vlugt T J H 2020 *Nanomaterials* **10** 293
[10] Jiang Q and Ward M D 2014 *Chem. Soc. Rev.* **43** 2066
[11] Carretero-Genevrier A, Puig T, Obradors X and Mestres N 2014 *Chem. Soc. Rev.* **43** 2042
[12] Gagliardi L and Pierre-Louis O 2018 *New J. Phys.* **20** 073050
[13] Dziadkowiec J, Zareeipolgardani B, Dysthe D K and Røyne A 2019 *Sci. Rep.* **9** 8948
[14] Downs R T and Palmer D C 1994 *Am. Mineral.* **79** 9–14 (ISSN 0003-004X)
[15] Frondel C 1962 *The system of mineralogy of James Dwight Dana and Edward Salisbury Dana, Yale University, 1837-1892. Vol. III, Silica Minerals* 7th (London and New York: John Wiley & Sons, Inc) 273–86
[16] Dera P, Lazarz J D, Prakapenka V B, Barkley M C and Downs R T 2011 *Phys. Chem. Miner.* **38** 517–29
[17] Pluth J J, Smith J V and Faber J Jr 1985 *J. Appl. Physics* **57** 1045–9
[18] Buckley P, Hargreaves N and Cooper S 2018 *Comm. Chem.* **49** 1–10
[19] Damby D E, Llewellin E W, Horwell C J, Williamson B J, Najorka J, Cressey G and Carpenter M 2014 *J. Appl. Crystallogr.* **47** 1205–15
[20] Tang C, Zhu J, Zhou Q, Wei J, Zhu R and He H 2014 *J. Phys. Chem. C* **118** 26249–57
[21] Sanyal M K, Datta A and Hazra S 2002 *Pure Appl. Chem.* **74** 1553
[22] Garg N and Sharma S M 2007 *J. Phys. Condens. Matter* **19** 456201
[23] Naranjo T, Cerrón F, Nieto-Ortega B, Latorre A, Somoza Á, Ibarra B and Pérez E M 2017 *Chem. Sci.* **8** 6037